



Prediction of the impact of support structures on the aerodynamic performance of large wind farms

Cite as: J. Renewable Sustainable Energy **11**, 063306 (2019); <https://doi.org/10.1063/1.5120602>

Submitted: 19 July 2019 . Accepted: 12 November 2019 . Published Online: 10 December 2019

 Lun Ma (马伦), Takafumi Nishino (西野貴文), and Antonios F. Antoniadis

COLLECTIONS

 This paper was selected as Featured



View Online



Export Citation



CrossMark

ARTICLES YOU MAY BE INTERESTED IN

Heat transfer across a fractal surface


The Journal of Chemical Physics **151**, 134705 (2019); <https://doi.org/10.1063/1.5115585>

The design and modification of a parabolic trough system for the hydrothermal liquefaction of waste


AIP Conference Proceedings **2126**, 120001 (2019); <https://doi.org/10.1063/1.5117619>

Nanoflow over a fractal surface

Physics of Fluids **28**, 082001 (2016); <https://doi.org/10.1063/1.4958975>



Sign up for topic alerts
New articles delivered to your inbox



Prediction of the impact of support structures on the aerodynamic performance of large wind farms

Cite as: J. Renewable Sustainable Energy **11**, 063306 (2019); doi: [10.1063/1.5120602](https://doi.org/10.1063/1.5120602)

Submitted: 19 July 2019 · Accepted: 12 November 2019 ·

Published Online: 10 December 2019




View Online



Export Citation



CrossMark

Lun Ma (马伦),^{1,a)}  Takafumi Nishino (西野貴文),² and Antonios F. Antoniadis¹

AFFILIATIONS

¹School of Aerospace, Transport and Manufacturing, Cranfield University, Cranfield, Bedfordshire MK43 0AL, United Kingdom

²Department of Engineering Science, University of Oxford, Oxford OX1 3PJ, United Kingdom

^{a)}E-mail: l.ma@cranfield.ac.uk

ABSTRACT

An extended theoretical model based on a two-scale coupled momentum balance method is proposed to estimate aerodynamic effects of wind turbine towers on the performance of both ideal (infinitely large) and more realistic (large but finite-size) wind farms. A key implication of the extended model is that a normalized support-structure drag, $(A_s/A) \times C_D^*$, where A and A_s are the rotor swept area and support-structure frontal projected area, respectively, and C_D^* is an effective support-structure drag coefficient, may play an important role in the design of future large wind farms. For the infinitely large case, the theoretical model shows that the optimal turbine spacing should increase with the value of $(A_s/A) \times C_D^*$, whereas for the large finite case, this also depends on an additional parameter describing the response characteristics of the atmospheric boundary layer to the total farm drag. To validate the theoretical model for the infinitely large case, Wall-Modeled Large-Eddy Simulations of a periodic array of actuator disks with and without support structures are conducted. The results show a reasonably good agreement (within 10% in the prediction of power) with the theoretical model.

Published under license by AIP Publishing. <https://doi.org/10.1063/1.5120602>

I. INTRODUCTION

Wind farm development is one of the most challenging multidisciplinary businesses today; nevertheless, the wind energy industry is rapidly expanding with no sign of stopping. Due to the advantage of the vast open sea, unconventionally large offshore wind farms are currently under construction. The well-known Hornsea offshore wind projects, for instance, plan to install more than 300 large multimegawatt wind turbines across a total area of 869 km².¹ It seems to be clear that the size of future offshore wind farms is going to be enormous. The sizes of not only the wind farm but also the wind turbines are increasingly large. The rotor diameter of the latest wind turbines varies between 160 and 200 m. In order to be able to support these gigantic rotors in the harsh offshore environment, the support structures are also becoming extra-large and strong. The majority of existing wind farms employ monopiles for the support structures; therefore, we consider the effects of such support structures in this study.

There are several studies on wind turbine support structures, in terms of structural integrity, manufacturing, transport, and some others; however, the effects of support structures on wind farm's aerodynamic performance have been less investigated to date. Due to the complexity of modeling, support structures are often excluded in farm-scale Computational Fluid Dynamics (CFD) studies.^{2,3} For example,

recent large-eddy simulation (LES) studies performed by both Chatterjee and Peet⁴ and Zhang *et al.*⁵ look into the potentials of “vertically staggered” wind farms but without modeling turbine support structures. On the other hand, single turbine research often considers modeling the entire wind turbine including the support structure. For example, Wu and Porté-Agel⁶ have carefully implemented and investigated the support structure aerodynamic effects in both wind tunnel tests and LES, where the wake of the tower has been clearly seen.

There are also some theoretical large wind farm models reported in the literature, for instance, the original “top-down” model of Frandsen⁷ and the later improvements of Calaf *et al.*⁸ and Meneveau.⁹ However, none of these models have included the impact of support structures explicitly. In the Frandsen model,⁷ the wind profile averaged horizontally across an infinitely large wind farm was considered to be split into two parts—the outer layer and the inner layer—and a constant stress was assumed within each layer. This was one of the earliest models for the interaction between a large wind farm and the atmospheric boundary layer (ABL). An enhanced top-down model was proposed later by Calaf *et al.*⁸ Using LES, they confirmed the existence of the two logarithmic layers. In addition, their LES results also showed that due to the significant effect of wake created by the turbine rotors, an intermediate region (wake layer) should be added between

the two logarithmic layers. Later on, Meneveau⁹ further improved the theoretical top-down model by taking into account the farm entrance effect accompanied by the internal boundary layer (IBL) development, making it possible to apply the model to large but finite-size wind farms.

This paper, which is an extension of an earlier conference paper by the authors,¹⁰ investigates the effect of support structures on the aerodynamic performance of large wind farms using the theoretical two-scale momentum model of Nishino¹¹ (also see the study by Nishino and Hunter¹²). This model combines a farm-scale momentum balance equation with the classic actuator disk theory, thereby predicting the power of an ideal large wind farm in a simple quasi-1D manner. Instead of modeling the wind profile explicitly, the Nishino model focuses on the change in the average wind velocity across the wind farm. This quasi-1D approach is a reasonable and robust approach when considering real “complex” (nonlogarithmic) background wind profiles that may be caused due to various meteorological reasons.¹³ The original Nishino model has been shown to agree reasonably well with several different types of numerical simulations of a periodic actuator disk array.^{13–16} The model was originally only for an ideal, infinitely large wind farm but has recently been extended for a large finite-size wind farm as well.¹⁷ Therefore, in this paper, we further extend this quasi-1D model by taking into account the aerodynamic impact of turbine support structures (towers). Using the extended model, we investigate how the support-structure drag may affect the optimal design of future large wind farms. In addition, a series of CFD simulations are conducted to validate this extended theoretical model.

II. THEORETICAL MODEL

A. Infinitely large wind farm

The original two-scale momentum model¹¹ (see Ref. 12 for a full description of the model) has been designed to predict the performance of ideal “infinitely large” wind farms. A constant streamwise pressure gradient is assumed as the only driving force of the atmospheric boundary layer (ABL). Two different steady ABLs are compared with each other: one is the “unperturbed” or “natural” ABL observed before farm construction, and the other is the “perturbed” ABL observed after farm construction; thereby, a farm-scale momentum balance equation is derived. The new modification proposed in this study is to add the drag force due to turbine support structures, D , into the momentum balance equation as follows:

$$\langle \tau_w \rangle S + T + D = \tau_{w0} S, \quad (1)$$

where $\langle \tau_w \rangle$ is the bottom shear stress (wind-induced shear stress on the land or sea surface, depending on whether the farm is onshore or offshore) averaged across the area S , which is the average land/sea surface area per each turbine, T is the thrust on each rotor, D is the drag due to its support structure (tower), and τ_{w0} is the natural bottom shear stress, i.e., the shear stress on the land/sea surface at the construction site before constructing the farm. The rotor thrust T and tower drag D are then represented using “local” thrust and drag coefficients C_T^* and C_D^* (i.e., based on a locally averaged wind speed) as

$$T = \frac{1}{2} \rho U_F^2 A \cdot C_T^*, \quad (2)$$

$$D = \frac{1}{2} \rho U_F^2 A_s \cdot C_D^*, \quad (3)$$

where ρ is the air density, A and A_s are the rotor swept area and the support-structure frontal projected area, respectively, and U_F is the average wind speed across the wind farm layer introduced in Ref. 11. This layer is typically two to three times as high as the turbine hub height; see Ref. 12 for further details.

Figure 1 shows a schematic of the flow scenarios considered in the theoretical model, reproduced (with minor modifications) from Ref. 11. It should be noted that, for the case of an infinitely large wind farm, the driving force observed after farm construction, Δp , is assumed to be equal to that observed before farm construction, Δp_0 (based on the assumption that the size of the atmospheric system creating a pressure gradient is also infinitely large), yielding the simple momentum balance Eq. (1) given earlier. For the case of a large finite-size wind farm to be discussed in Subsection II B, this assumption will be removed.

Following the original two-scale momentum model,¹¹ C_T^* is modeled using the classical actuator disk theory. This may appear to be a strong simplification but tends to yield a good agreement with 3D numerical simulations of a fully staggered array of actuator disks with a wide range of interturbine spacings from $6d \times 6d$ to $14d \times 14d$,^{14,15} where d is the rotor diameter. Note, however, that this simple representation of C_T^* may need to be replaced by a more advanced model, such as the one proposed recently in Ref. 18 if an even smaller turbine spacing is of interest. Eventually, the momentum balance Eq. (1) is transformed into the following nondimensional form:

$$\left(4\alpha(1 - \alpha) + \frac{A_s}{A} C_D^* \right) \frac{\Lambda}{C_{f0}} \beta^2 + \beta^\gamma - 1 = 0, \quad (4)$$

where $\alpha = U_T/U_F$ (U_T is the average wind speed across A), $\beta = U_F/U_{F0}$ (U_{F0} is the natural farm-layer wind speed observed before farm construction), $\Lambda = A/S$ is the farm density, $C_{f0} = \tau_{w0}/\frac{1}{2}\rho U_{F0}^2$ is a natural friction coefficient, and $\gamma = \log_\beta(\langle \tau_w \rangle/\tau_{w0})$ is an empirical parameter to model the wall shear stress ratio $\langle \tau_w \rangle/\tau_{w0}$. The value of γ is typically between 1.5 and 2,^{14,15} but in the present study, we assume $\gamma = 2$ as this value is expected for an ideal case.¹¹ Since Eq. (4) can be solved to obtain β as a function of α [for a given set of model inputs: γ , Λ/C_{f0} , and $(A_s/A)C_D^*$], we can calculate the power coefficient of a turbine in the farm,

$$C_P = \frac{\text{Power}}{\frac{1}{2}\rho U_{F0}^3 A} = \frac{T U_T}{\frac{1}{2}\rho U_{F0}^3 A} = \frac{U_F^2 U_T}{U_{F0}^3} \cdot 4\alpha(1 - \alpha) = \beta^3 \cdot 4\alpha^2(1 - \alpha). \quad (5)$$

In addition, the normalized power density, η , can be defined¹¹ as an alternative representation of the farm performance,

$$\eta = \frac{\text{Power}}{\tau_{w0} U_{F0} S} = \frac{\frac{1}{2}\rho U_{F0}^3 A \cdot C_P}{\tau_{w0} U_{F0} S} = \Lambda \cdot \frac{1}{C_{f0}} \cdot C_P. \quad (6)$$

Some example solutions are presented below to show how the model predicts the effect of support structures on the farm performance and then an optimal farm density to maximize the performance. Traditional turbine spacing for offshore wind farms is around $7d$ and could potentially be as large as $15d$.¹⁹ Furthermore, for an average wind speed of 10 m/s, for example, the natural friction coefficient of the sea surface can be assumed to be around 0.002 (depending on

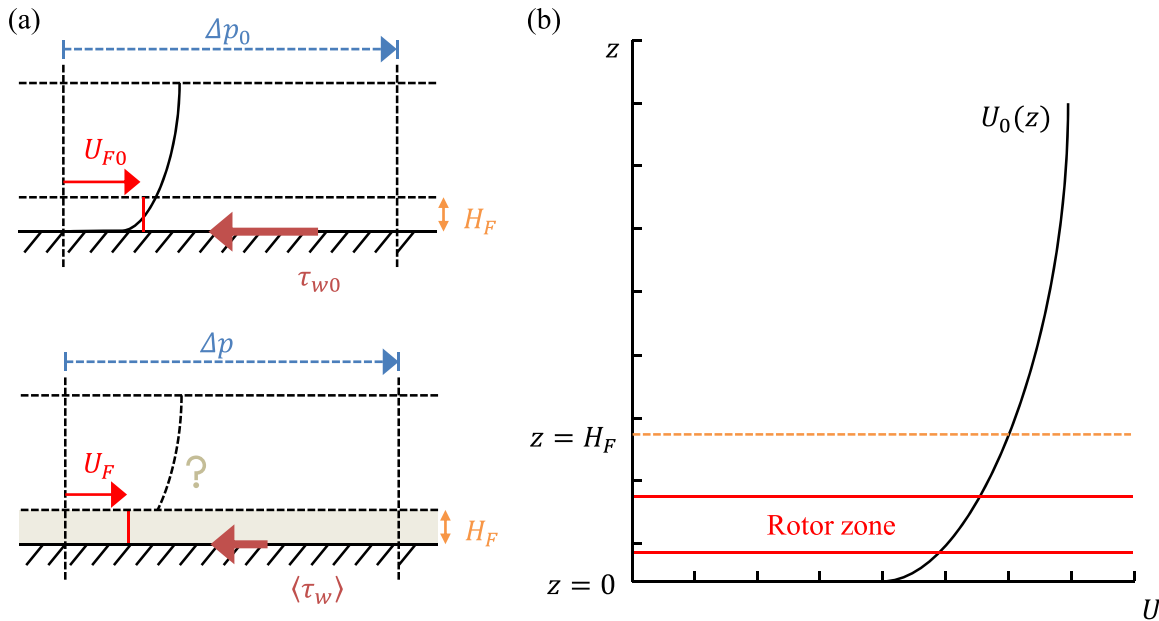


FIG. 1. Schematic of the two-scale momentum model: (a) fully developed boundary layer before and after farm construction, (b) nominal farm-layer height, H_F . Reproduced from Ref. 11 with minor modifications.

various wind-wave interaction parameters).²⁰ Therefore, we presume that a typical range of effective farm densities (Λ/C_{f0}) of offshore wind farms should be around 2–8, assuming an interturbine distance of around $7d$ – $14d$. It is also worth noting that some recent studies suggest that an even shorter interturbine distance may be beneficial for a wind farm with wake control, e.g., Ref. 21. Hence, in the below example, we consider a wider range of 0–10 for the effective farm density.

For the most common monopile-type foundation design for large offshore wind turbines (with a diameter of typically about 2–6 m),²² the drag coefficient is expected to be around 0.6 (from that for a

circular cylinder under relevant Reynolds number conditions²³), and hence, the value of the normalized support-structure drag $[(A_s/A)C_D^*]$ is expected to be up to about 0.1 in most cases (depending on the area ratio A_s/A). Note that, strictly speaking, the value of C_D^* [defined as in Eq. (3) using the farm-average wind speed U_F instead of an upstream wind speed] can be different from the value of a commonly used drag coefficient (defined using an upstream wind speed). However, this difference is expected to be small unless the turbines are perfectly aligned with the wind direction to cause a significant level of direct wake interference.¹² Figure 2 shows the variations of β and η against the local axial

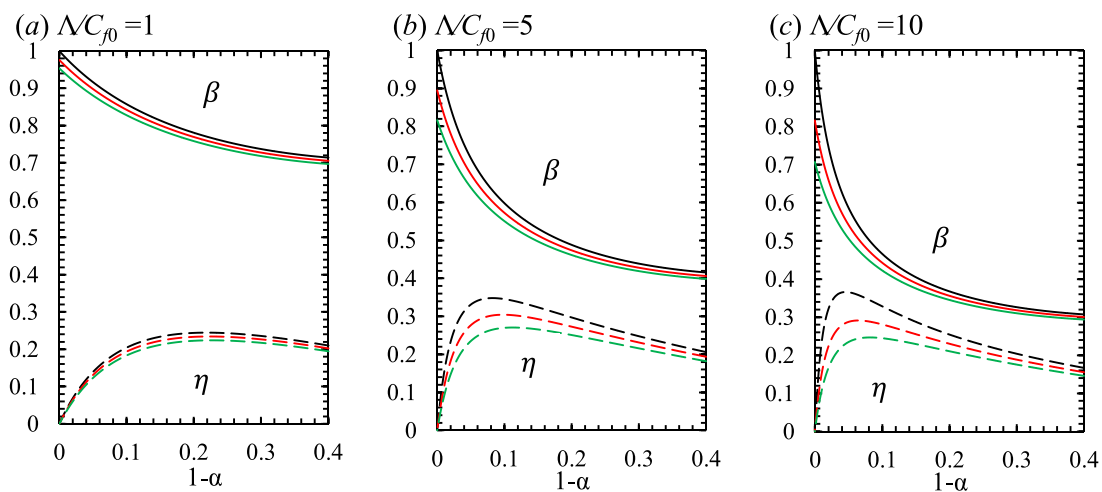


FIG. 2. Effects of support-structure drag on the performance of infinitely large wind farms: solid and dashed lines show β and η , respectively, and $(1 - \alpha)$ is the local axial induction factor of each rotor. Black: $(A_s/A)C_D^* = 0$; red: $(A_s/A)C_D^* = 0.05$; and green: $(A_s/A)C_D^* = 0.1$.

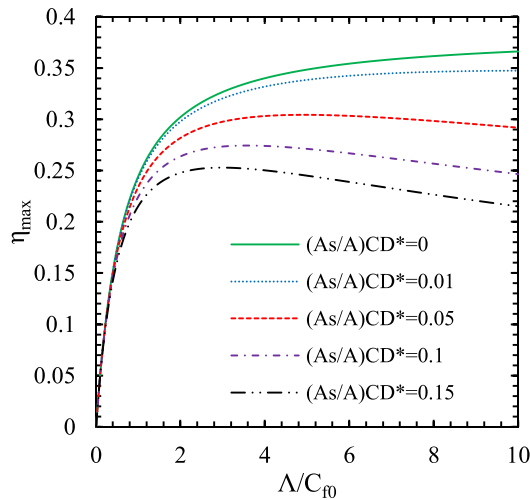


FIG. 3. The maximum normalized power density η_{\max} (for infinitely large wind farms) against the effective farm density Λ/C_{f0} for various normalized support-structure drag values $(A_s/A)C_D^*$.

induction factor $(1 - \alpha)$, for three infinitely large wind farms with Λ/C_{f0} values of 1, 5, and 10, with three $(A_s/A)C_D^*$ values of 0, 0.05, and 0.1, respectively. The overall wind farm performance is hardly influenced by the support structures when the effective farm density is small ($\Lambda/C_{f0} = 1$). However, as the farm density increases, the support-structure effect becomes more obvious; for example, at $\Lambda/C_{f0} = 5$, the maximum power density for $(A_s/A)C_D^* = 0.1$ ($\eta_{\max} \approx 0.27$ at $\alpha \approx 0.89$) is more than 20% lower than that for $(A_s/A)C_D^* = 0$, i.e., for the case without support structures ($\eta_{\max} \approx 0.35$ at $\alpha \approx 0.92$).

Figures 3 and 4 summarize the effects of farm density and support-structure drag on the maximum farm performance. When the support-structure drag is zero, this model goes back to the original

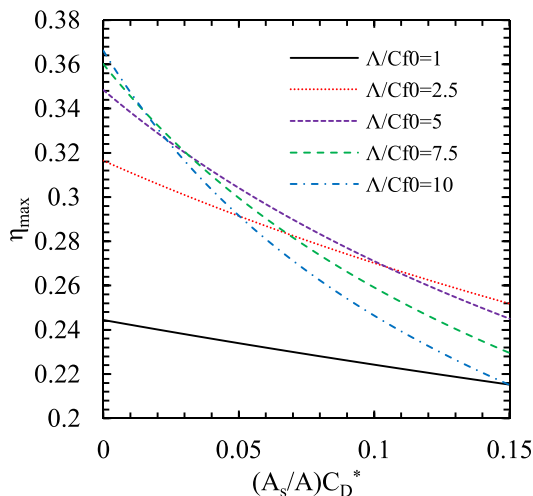


FIG. 4. The maximum normalized power density η_{\max} (for infinitely large wind farms) against the normalized support-structure drag $(A_s/A)C_D^*$ for various effective farm densities Λ/C_{f0} .

two-scale coupled momentum model,¹¹ in which the maximum power density η_{\max} always increases with the effective farm density Λ/C_{f0} and approaches asymptotically to $\eta_{\max} = 0.385$. However, when the support-structure effect is considered, the power density increases with the farm density only up to an optimal value, above which the power decreases (Fig. 3). Importantly, the impact of support-structure drag on the maximum power density becomes more and more significant as the farm density increases (Fig. 4). This is basically because the optimal rotor thrust decreases,¹⁴ and therefore, the relative importance of support-structure drag increases as the farm density increases. It should be noted that, while the rotor thrust can be reduced or optimized by changing the rotor operating conditions, the support-structure drag cannot be reduced unless the design of support structures is changed. This implies that the farm density of a very large wind farm should be optimized by taking into account the design of support structures. This can be seen more clearly from Fig. 5, which shows how the optimal values of the effective farm density (Λ/C_{f0}) and rotor resistance [$K = T/(\frac{1}{2}\rho U_T^2 A) = 4(1 - \alpha)/\alpha$] change with the normalized support-structure drag $[(A_s/A)C_D^*]$. Also plotted in this figure are the maximum normalized power density (η_{\max}) values obtained from such an optimization.

B. Large finite-size wind farm

A simple yet effective extension of the original two-scale coupled momentum model has recently been proposed by Nishino.¹⁷ The main purpose of this extension was to overcome a major assumption in the original model, which was that the streamwise pressure gradient (given as the only driving force of the flow over the farm site) was the same before and after wind farm construction. This assumption seems to be reasonable when considering an ideal, infinitely large wind farm but may not be appropriate for a large finite-size wind farm, where the reduction of wind speed may occur even upstream of the entire farm,²⁴ and hence, the farm may experience a larger streamwise pressure gradient than that observed before farm construction.^{12,17}

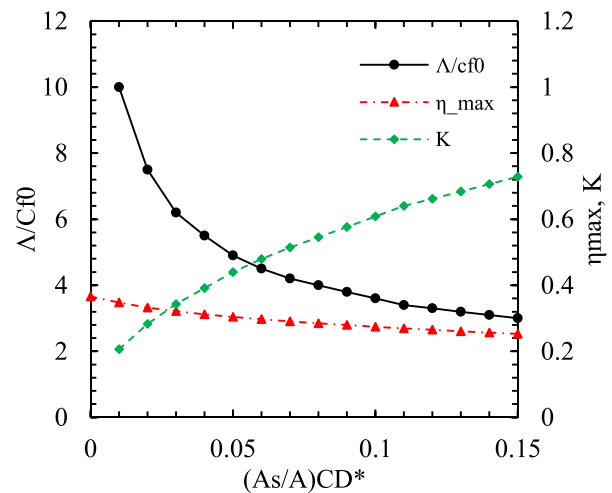


FIG. 5. The optimal values of effective farm density Λ/C_{f0} , rotor resistance $K (= \frac{4(1-\alpha)}{\alpha})$, and the maximum normalized power density η_{\max} (for infinitely large wind farms) plotted against the normalized support-structure drag $(A_s/A)C_D^*$.

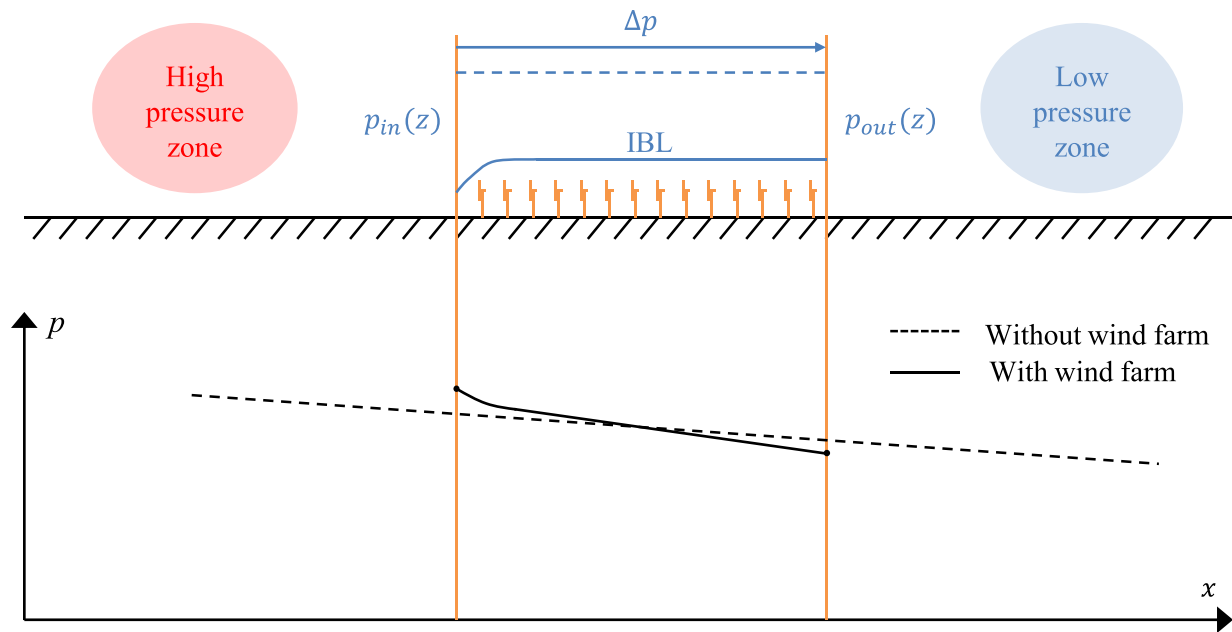


FIG. 6. Schematic of an additional pressure gradient induced by a large finite-size wind farm. Reproduced from Ref. 17 with modifications.

Figure 6 shows a schematic of this additional pressure gradient induced by a large finite-size wind farm, where $p_{in}(z)$ and $p_{out}(z)$ are the pressure (as a function of the height, z) at the inlet and outlet of the farm site, respectively. If we consider a large control volume containing the entire farm and the internal boundary layer (IBL) developing over it and assume that the momentum exchange through the top surface of this control volume is negligibly small, then we may still consider the (vertically averaged) pressure difference, Δp , as the only driving force of the flow over the farm. Therefore, by considering the (steady) momentum balance before and after farm construction separately and then combining the two, we obtain the following farm-scale momentum equation:

$$\langle \tau_w \rangle S + T + D = \frac{\Delta p}{\Delta p_0} \tau_{w0} S. \quad (7)$$

Compared to Eq. (1), it can be seen that the pressure ratio, $\Delta p_0/\Delta p$, has been added to the right-hand side to take into account the change in the driving force before and after farm construction. Note that, in reality, the momentum exchange at the top of the control volume in Fig. 6 may not be negligibly small, but this effect can also be added to the right-hand side of Eq. (7) in a similar manner if necessary. It should also be noted that an implicit assumption here is that the IBL develops immediately at the entrance of the farm (i.e., the farm entrance effect is ignored) so that all turbines in the farm experience the same flow conditions; in reality, the IBL may or may not reach a fully developed state depending on atmospheric stability conditions.²⁵ Following the same procedure as the infinitely large farm case presented earlier, Eq. (4) is now rewritten for the finite-size farm case as

$$\left(4\alpha(1-\alpha) + \frac{A_s}{A} C_D^* \right) \frac{\Lambda}{C_{f0}} \beta^2 + \beta' - 1 = \frac{(\Delta p - \Delta p_0)}{\Delta p_0}. \quad (8)$$

The right-hand side of Eq. (8), namely, the farm-induced pressure term,¹⁷ depends on various environmental conditions, such as geographical characteristics of the farm site, atmospheric conditions, and the ratio of the farm size to the size of the relevant atmospheric system driving the flow. However, for a given environment, this term should primarily depend on the farm-scale flow reduction factor β . In fact, the CFD results presented in Ref. 17 show that the farm-induced pressure term tends to increase approximately linearly with the farm-scale flow induction factor $(1 - \beta)$, making it possible to model this term as

$$\frac{(\Delta p - \Delta p_0)}{\Delta p_0} = \zeta(1 - \beta), \quad (9)$$

where ζ is an “environment-dependent” parameter, which requires an empirical estimation for a given wind farm. The estimation of this parameter ζ is outside the scope of this paper; however, there is an ongoing study using a numerical weather prediction model with a single volume of momentum sink (representing an entire wind farm rather than individual turbines) to determine this parameter. In short, this parameter depends on how easily or not easily the flow approaching a large wind farm is deflected by the farm itself and is therefore closely related to the so-called wind farm blockage effect.²⁶

Some example results of the extended model are shown in Figs. 7–9 with three ζ values of 2, 5, and 10. Although there are no conclusive data supporting the choice of these three values at this stage, the CFD simulation results presented in Ref. 17 suggest that a typical value of this environmental parameter may vary between 5 and 10 depending on the natural roughness length of the farm site (e.g., onshore or offshore). Figure 7 shows a similar plot to Fig. 3 but now for finite-size wind farms. One key difference from the infinitely large case presented earlier is that the maximum normalized power density (η_{\max}) no

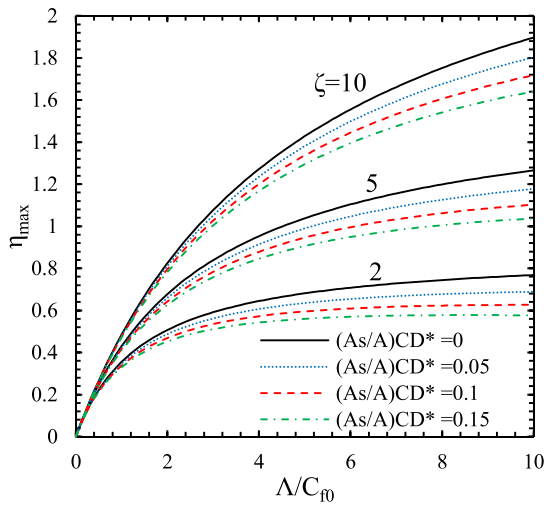


FIG. 7. The maximum normalized power density η_{\max} against the effective farm density Λ/C_{f0} for various normalized support structure drag values $(A_s/A)C_D^*$ and environmental parameters ζ .

longer has a clear peak point at $\Lambda/C_{f0} < 10$. When ζ equals 2, the power density tends to be maximized around $\Lambda/C_{f0} = 10$; however, for ζ equal to 5 and 10, the power density is maximized at $\Lambda/C_{f0} > 10$, meaning that the optimal farm density (to maximize the power density) increases with the response strength of the driving force of flow over the farm (which is represented by ζ in this model). It should be remembered that Λ/C_{f0} higher than 10 may be unrealistic (at least from the current industrial standard), and also, as noted in Subsection II A, the theoretical model may become invalid at such a high Λ/C_{f0} value. Nevertheless, these results show that the support structure drag may still affect the power density substantially, in a realistic range of Λ/C_{f0} values, not only for infinitely large but also for large finite-size

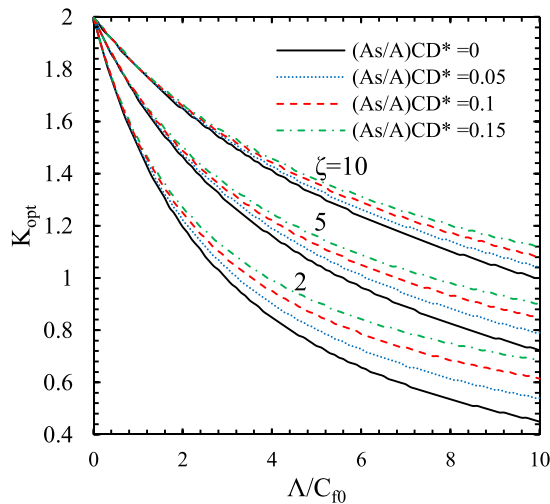


FIG. 8. The optimal rotor resistance K_{opt} against the effective farm density for various Λ/C_{f0} normalized support-structure drag $(A_s/A)C_D^*$ and environmental parameter ζ .

wind farms (regardless of the value of ζ). The optimal rotor resistance (K_{opt}) plot in Fig. 8 also shows the importance of the support structure drag for all three different ζ cases, but especially when ζ is small ($\zeta = 2$ in this case). Finally, Fig. 9 shows the effects of support structure drag on the maximum power coefficient of each turbine ($C_{p\max}$) for the three different ζ cases. The results for $(A_s/A)C_D^* = 0$ (i.e., without tower) agree with the previous study,¹⁷ and as expected, the support structure drag tends to reduce $C_{p\max}$. Overall, these results show that both ζ and $(A_s/A)C_D^*$ tend to affect the power of large finite-size wind farms substantially.

III. CFD SIMULATIONS

Due to the wide range of parameters involved, the theoretical results presented in Sec. II cannot be entirely verified using CFD simulations; hence, only some example cases are simulated focusing on the impact of support structures. The CFD model employed is a Wall-Modeled Large-Eddy Simulation (WMLES) of a pressure-driven ABL coupled with localized streamwise momentum sinks representing turbine rotors and support structures. The simulations are performed for horizontally periodic staggered arrays of turbines with and without support structures to be compared with the theoretical results for infinitely large wind farms.

A. Computational domain and flow conditions

Unlike the previous studies^{11,14} that used Reynolds-averaged Navier-Stokes (RANS) simulations of a single turbine in a small periodic domain, in this study, we consider four turbines in a larger periodic domain as shown in Fig. 10. The turbine spacing is $L_x \times L_y = 7d \times 7d$ (with a lateral displacement of $\Delta_y = 3.5d$ for the staggered arrangement), and the height of the domain (L_z) is $10d$ with a clearance of $0.5d$ between the ground and rotors; hence, the size of the computational domain is $2L_x \times 2L_y \times L_z = 14d \times 14d \times 10d$. The rotor diameter d is 100 m. This configuration is identical to one of the cases employed in the previous RANS study by Zapata *et al.*,¹⁴ except

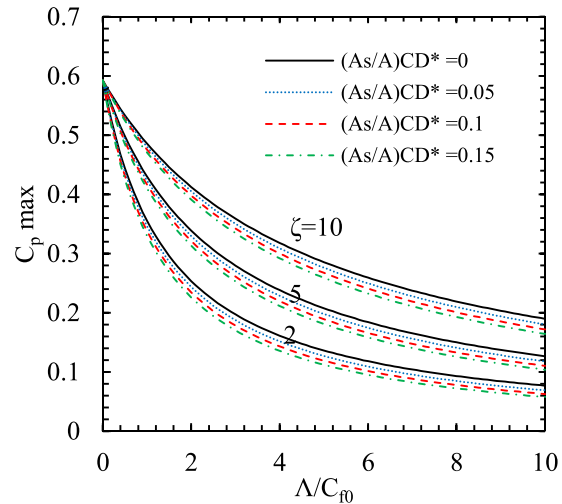


FIG. 9. The maximum C_p value against the effective farm density Λ/C_{f0} for various normalized support structure drag values $(A_s/A)C_D^*$ and environmental parameters ζ .

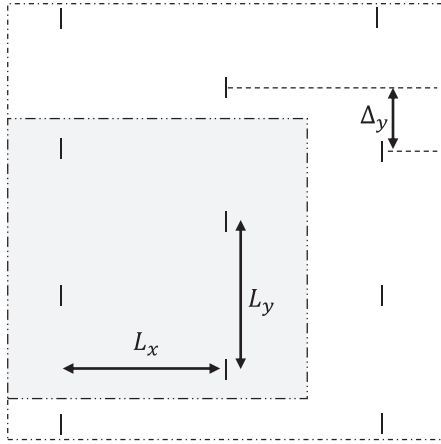


FIG. 10. Schematic of turbine arrangements (with the computational domain in gray).

that four turbines are simulated (instead of one) in the present WMLES study. Note that, compared to some recent LES studies of infinitely large wind farms such as Refs. 27 and 28, the current computational domain is still relatively small (due to the availability of our computational resources), and hence, the influence of large-scale coherent structures (that may cause wake meandering) cannot be fully captured in our simulations. However, the effects of such large-scale coherent structures are outside the scope of the present study (as the steady theoretical model does not take account of such effects either).

Periodic boundary conditions are applied to both streamwise and lateral directions. The top of the domain is treated as a symmetry boundary, whereas the bottom of the domain is treated as a rough wall boundary; more details will be explained in Subsection III B. As with the previous study by Zapata *et al.*,¹⁴ the air flow is driven by a constant pressure gradient. This pressure gradient value is calculated from an “empty box” simulation, in which a constant mass flow rate (corresponding to a vertically averaged wind speed of 10 m/s for the entire domain) is given in order to obtain the pressure gradient for a fully developed boundary layer flow without any turbines.

B. Computational methods

All calculations are conducted using the commercial CFD solver “ANSYS FLUENT 17.2.”²⁹ The original version of the Detached-Eddy Simulations (DES) approach using the Spalart-Allmaras model (often referred to as DES97) is employed as a mean to conduct simple WMLES,^{30,31} i.e., the flow in the vicinity of the bottom boundary is treated as in RANS and the rest of the domain is treated as in LES. The reason for employing DES97, instead of more advanced DES approaches, is that the thickness of the RANS layer can be fixed and controlled explicitly by adjusting near-wall mesh resolutions. As will be described later, we employ a uniform horizontal mesh resolution of 10 m near the bottom boundary for the entire domain; hence, the thickness of the RANS layer is 6.5 m in this study (as the DES model coefficient $C_{DES} = 0.65$ in DES97). In addition, similar to the previous RANS study,¹⁴ the effect of bottom roughness is modeled using a

modified wall function for “fully rough” walls available in FLUENT²⁹ as follows:

$$\frac{U_p u^*}{\tau_w / \rho} = \frac{1}{\kappa} \ln \left(E \frac{\rho u^* y_p}{\mu} \right) - \Delta B, \quad (10)$$

$$u^* = C_\mu^{0.25} k^{0.5}, \quad (11a)$$

$$\Delta B = \frac{1}{\kappa} \ln(1 + C_s k_s^+), \quad (11b)$$

$$k_s^+ = \frac{\rho k_s u^*}{u_\tau}, \quad (12a)$$

$$u_\tau = \sqrt{\frac{\tau_w}{\rho}}, \quad (12b)$$

where U_p is the velocity at the centroid of the wall-adjacent cell (i.e., $y = y_p$). The two roughness parameters, namely, the nominal “sand-grain” type roughness height k_s and the roughness constant C_s , are set to 1 m and 0.5, respectively [this corresponds to an aerodynamic roughness length of $z_0 = 0.051$ m since $k_s = (E/C_s)z_0$,³² where $E = 9.793$ is an empirical value used in FLUENT²⁹]. The density and viscosity of the working fluid (air) are constant in this study: $\rho = 1.225$ kg/m³ and $\mu = 1.789 \times 10^{-5}$ kg/m s, respectively.

The effects of both turbine rotors and support structures are modeled as streamwise momentum losses, i.e., both rotors and support structures are modeled as stationary permeable (or porous) surfaces of zero thickness with a momentum loss factor (K for the rotors and K_s for the support structures), by which their resistance can be changed. Specifically, the instantaneous momentum loss is calculated as

$$M_x = K_{(s)} \cdot \frac{1}{2} \rho u^2, \quad (13)$$

where u is the instantaneous streamwise velocity. Since the time-averaged rotor thrust and support-structure drag can be obtained as $T = \int M_x dA$ and $D = \int M_x dA_s$, it is possible to calculate the local rotor thrust coefficient C_T^* and local support-structure drag coefficient C_D^* as

$$C_T^* = \frac{T}{\frac{1}{2} \rho U_F^2 A} = K \frac{\int u^2 dA}{U_F^2 A}, \quad (14)$$

$$C_D^* = \frac{D}{\frac{1}{2} \rho U_F^2 A_s} = K_s \frac{\int u^2 dA_s}{U_F^2 A_s}. \quad (15)$$

However, for the purpose of comparison with the theoretical model, which is essentially for the time-averaged flow field and does not consider any velocity fluctuations in time, here we calculate C_T^* and C_D^* directly from the time-averaged flow field, i.e.,

$$C_T^* = K \frac{U_T^2}{U_F^2}, \quad (16)$$

$$C_D^* = K_s \frac{U_s^2}{U_F^2}, \quad (17)$$

where U_T and U_s are the spatial- and time-averaged streamwise velocities over the rotor area A and the support-structure area A_s , respectively. Note that the values of C_T^* and C_D^* calculated from Eqs. (16)

TABLE I. Summary of support structure characteristics.

Case	K_s	C_D^*	$(A_s/A)C_D^*$
1	0	0	0
2	0.542	0.270	0.0321
3	1.129	0.448	0.0533
4	1.422	0.505	0.0600
5	1.716	0.537	0.0640
6	4	0.739	0.0879
7	5	0.774	0.0921

and (17) are a little different from those from Eqs. (14) and (15) since, in general, $\overline{u^2} > \overline{u}^2$; however, we ignore this small difference in this study. Similarly, since the time-averaged rotor power can be obtained as $P = \int M_x u dA$, it is possible to calculate the rotor power coefficient C_P as

$$C_P = \frac{P}{\frac{1}{2} \rho U_{F0}^3 A} = K \frac{\int u^3 dA}{U_{F0}^3 A}, \quad (18)$$

but again, for the purpose of comparison with the steady theoretical model, here we calculate C_P as

$$C_P = K \frac{U_T^3}{U_{F0}^3} = K \alpha^3 \beta^3. \quad (19)$$

In order to simulate the support-structure drag in a simplified manner, we consider that the support structure is located only below each rotor disk (as shown later in Fig. 12). The areas of the rotor disk and support structure are fixed for all cases in this study (with a ratio of $A_s/A = 0.119$), which means that only the value of K_s needs to be modified to vary the support-structure drag. Here, we consider seven different K_s values as summarized in Table I. Two of the K_s values (0.542 and 1.716) were selected based on our initial speculation that these two values would result in $C_D^* = 0.42$ and 0.84 (and hence $(A_s/A)C_D^* = 0.05$ and 0.1) if a theoretical relationship $C_D^* = K_s \left(\frac{4}{4+K_s} \right)^2$ (following the actuator disk theory) was satisfied; however, we eventually found that the actual C_D^* values obtained from the simulations were smaller than those initial speculations, as can be seen from Table I. The difference could be due to the coarse mesh resolution for the tower as well as to the effects of the surroundings (ground and rotor disks) that are not

considered in the actuator disk theory. Nevertheless, this is not a major issue in this study since the aim here is to make a comparison of wind farm performance between CFD and the theoretical model for a given $(A_s/A)C_D^*$ (and not for a given K_s or for a given tower design). In other words, the present approach (using a porous plate model with a coarse mesh) may not be sufficient to predict C_D^* accurately for a given K_s or for a given tower design, but this is not the main concern of this study.

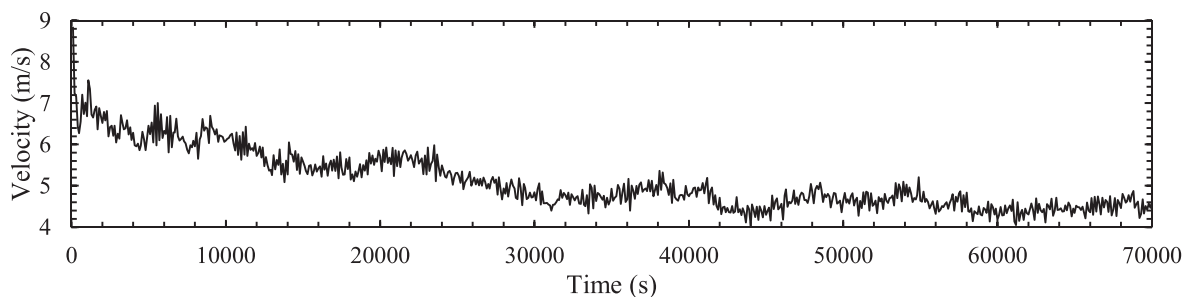
The numerical methods employed are nominally second-order accurate in space and time, using a bound central difference scheme for spatial discretization of the momentum equations and a second-order implicit scheme for temporal discretization. The SIMPLE algorithm is used for pressure-velocity coupling. A constant time step size of 0.1 s is adopted with 10 iterations at each time step. Each farm simulation has been run for 600 000 time steps initially, followed by another 100 000 time steps to calculate the time-averaged results. Figure 11 shows an example of the time history of the streamwise velocity averaged over the four disks, showing that the simulation has been run long enough to obtain reliable time-averaged results. We have run for an additional 100 000 time steps (from 70 000 s to 80 000 s) to take another time-average of the velocity and confirmed that the difference from the original time-average value is about 2.03%.

C. Computational mesh

Multiblock structured meshes are employed in this study. A 2D mesh for a cross-sectional (y - z) plane is generated first and then extruded to the streamwise direction (x) to form the 3D mesh with hexahedral cells. An “O-grid” mesh topology is used inside and around the rotor disk, to distribute cells along the edge of the disk. The smallest mesh spacing is 1 m, which is for the first cells above the bottom surface in the vertical (z) direction. For the horizontal (x and y) directions, however, a constant spacing of 10 m is employed for the entire domain (Fig. 12). The total number of cells is 1.3×10^6 .

D. Results and discussion

Table II compares the results of “empty box” simulations using WMLES and RANS. For RANS, we have tested the k - ω SST (Menter’s Shear Stress Transport) model as well as the Spalart-Allmaras model for comparison. Also presented for comparison are results from the previous RANS study by Zapata *et al.*¹⁴ using the Standard k - ε model. The (spatial- and time-averaged) natural bottom shear stress τ_{w0} obtained from WMLES is about 14% smaller than that from the Spalart-Allmaras RANS result. This trend, where WMLES using DES97 tends to yield a smaller wall shear stress, is in agreement with

**FIG. 11.** Example of the time history of streamwise velocity averaged over four disks (the sampling rate is every 100 s).

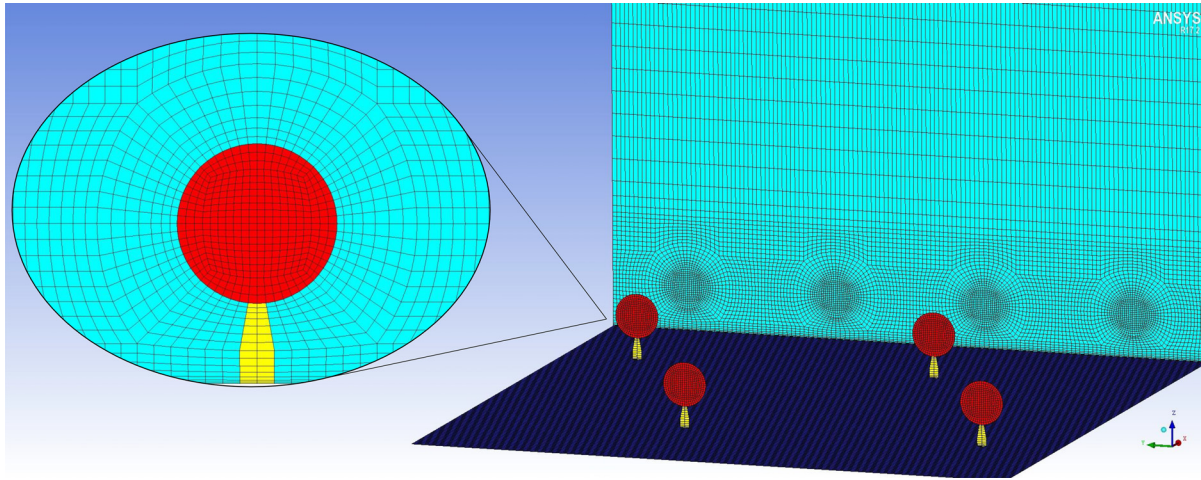


FIG. 12. Cross-sectional mesh for the rotor disk (red), tower (yellow), and surrounding area (light blue).

TABLE II. Comparison of empty box results between WMLES and RANS.

	τ_{w0} (Pa)	Pressure gradient (Pa/m)	U_{F0} (m/s)	H_F/d	Λ/C_{f0}
WMLES	0.1785	-1.785×10^{-4}	8.89	2.8	4.35
Spalart-Allmaras (RANS)	0.2081	-2.081×10^{-4}	8.55	2.6	3.45
$k-\omega$ SST (RANS)	0.2364	-2.364×10^{-4}	8.59	2.6	3.06
Standard $k-\varepsilon$ (RANS) ¹⁴	0.2597	-2.597×10^{-4}	8.34	2.6	2.63

Ref. 30. It should also be noted that the quantitative accuracy of the prediction of τ_{w0} for a given roughness height is not our primary concern because the theoretical results to be compared with these CFD results for validation (such as the power coefficient C_p) are given as a function of Λ/C_{f0} (not as a function of the roughness height).

Key results from the farm simulations (using WMLES) are summarized in Table III, where C_p is calculated using Eq. (19). It can be seen that the turbine support structures have a minor effect on the value of γ , which is slightly higher than that obtained in the previous RANS study¹⁴ but still approximately 10% lower than $\gamma = 2$, which was considered as a theoretical upper limit in the two-scale momentum model.¹¹

TABLE III. Summary of farm simulation results ($H_F = 280$ m, $U_{F0} = 8.89$ m/s).

Case	K	α	β	τ_w/τ_{w0}	γ	C_p
1	0.5	0.880	0.598	0.402	1.77	0.0728
2	0.5	0.873	0.598	0.397	1.80	0.0713
3	0.5	0.872	0.572	0.374	1.76	0.0622
4	0.5	0.870	0.569	0.365	1.79	0.0605
5	0.5	0.876	0.572	0.365	1.80	0.0627
6	0.5	0.883	0.569	0.363	1.80	0.0634
7	0.5	0.882	0.550	0.341	1.80	0.0570

Figure 13 shows an example of instantaneous velocity contours on three different places, visualizing the wakes of the turbine rotors and support structures. More details of the instantaneous flow field are compared between three different cases in Figs. 14 and 15; the former is on a horizontal plane at the tower midheight, and the latter is at the rotor hub-height. It can be seen that a narrow but increasingly clear wake pattern is visible behind each tower as the tower drag increases (Fig. 14), even though the towers have been modeled in a rather simplified manner. In addition, not only at the tower midheight but also at the rotor hub-height (Fig. 15), the streamwise velocity is (on average) slowed down due to the high support-structure drag. This can be seen more clearly in Fig. 16, which shows a comparison of time-averaged velocity profiles behind one of the turbines between the cases with and without the tower. In addition to creating the narrow wake, the tower also tends to cause an effect similar to the local blockage effect,³³ i.e., the acceleration of flow below the rotor (that happens if there is no tower) is prevented by the tower; such a blockage effect is not accounted for in the theoretical model presented in Sec. II.

Now, we compare the values of α , β , and C_p obtained from the CFD simulations with the theoretical model predictions. In the theoretical model, α is constant at 8/9 when the rotor resistance K is fixed at 0.5 [because $K = 4(1 - \alpha)/\alpha$]; meanwhile, the CFD simulations show nearly constant α values of slightly less than 8/9 (Fig. 17, left). Both the CFD and theoretical model also predict the same trend that β decreases as the support-structure drag increases (Fig. 17, right); the difference in β is about 3% at the maximum, which is similar to that

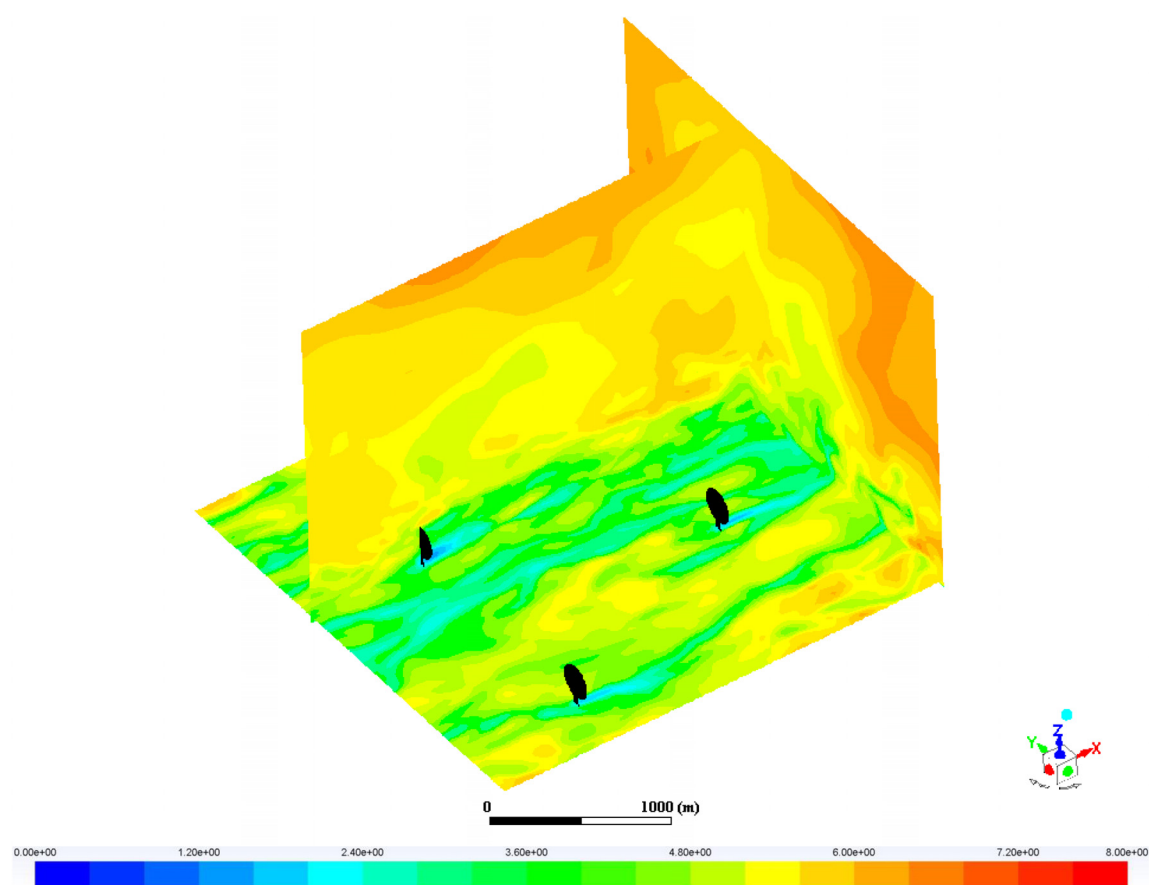


FIG. 13. Instantaneous streamwise velocity contours (m/s) on the horizontal plane at the tower midheight, streamwise vertical plane across the center of a turbine, and the spanwise vertical plane at the downstream end of the domain (taken at the last time step). Case 6 (with towers, $K_s = 4$).

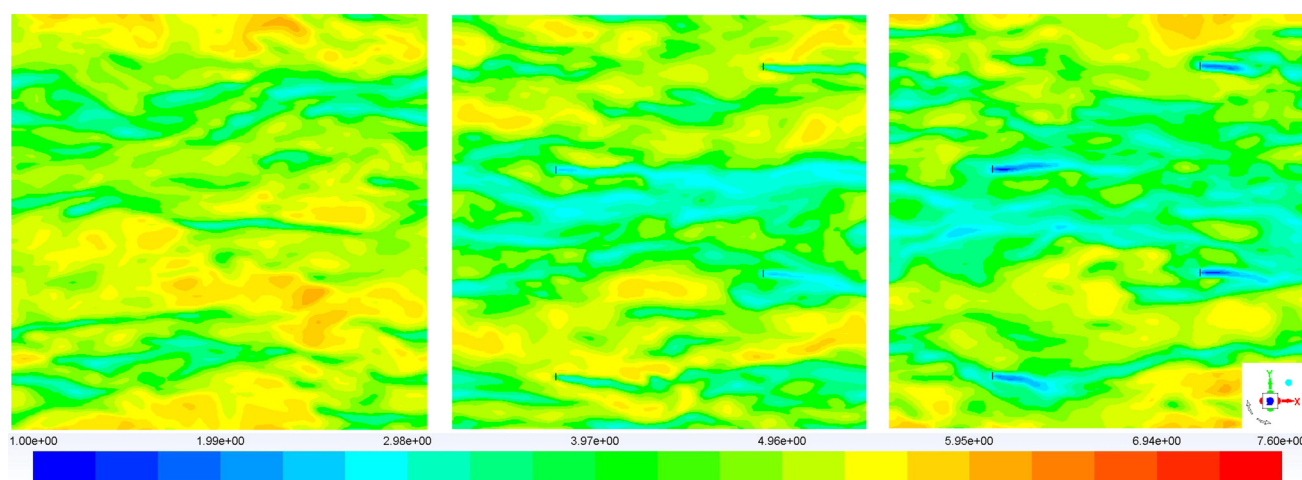


FIG. 14. Contours of instantaneous streamwise velocity (m/s) at the tower midheight (taken at the last time step). Left: Case 1 (no towers, $K_s = 0$), middle: Case 5 (with towers, $K_s = 1.716$); right: Case 6 (with towers, $K_s = 4$).

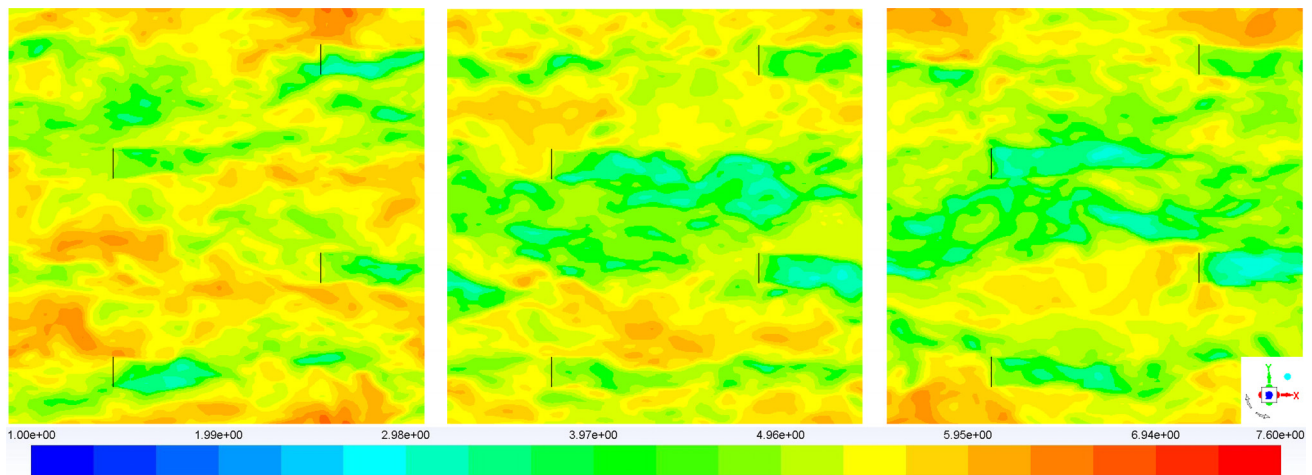


FIG. 15. Contours of instantaneous streamwise velocity (m/s) at the rotor hub-height (taken at the last time step). Left: Case 1 (no towers, $K_s = 0$), middle: Case 5 (with towers, $K_s = 1.716$), and right: Case 6 (with towers, $K_s = 4$).

found in the previous RANS study¹⁴ (where the discrepancy was less than 3% for the case without towers). Finally, the values of C_p obtained from the present CFD simulations are also in good agreement with the theoretical model predictions, showing the same trend that C_p decreases as the support-structure drag increases (Fig. 18). The values predicted by CFD are somewhat lower than the theoretical predictions, resulting from the slight differences in α and β . The maximum difference in C_p is about 10%, which is still reasonably good, considering the complexity of the 3D unsteady flow field simulated by CFD and the simplicity of the steady quasi-1D theoretical model.

Finally, it should be noted that the present study has considered only the staggered array and not the aligned array of turbines. As demonstrated by earlier RANS studies (for cases without support

structures),^{11,14} when the turbines are aligned perfectly with the wind direction, the value of C_p may further decrease due to the direct interference of rotor wakes, and hence, the difference from the quasi-1D theoretical model tends to increase. However, such a perfectly aligned situation is not very common in real wind farms.

IV. CONCLUSIONS

An extended two-scale coupled momentum model has been proposed in this study to estimate potential impacts of turbine support-structure drag on the aerodynamic performance of (i) an ideal, infinitely large wind farm and (ii) a more realistic, large but finite-size wind farm. A key implication of the proposed model is that the support structures may have an increasingly important influence

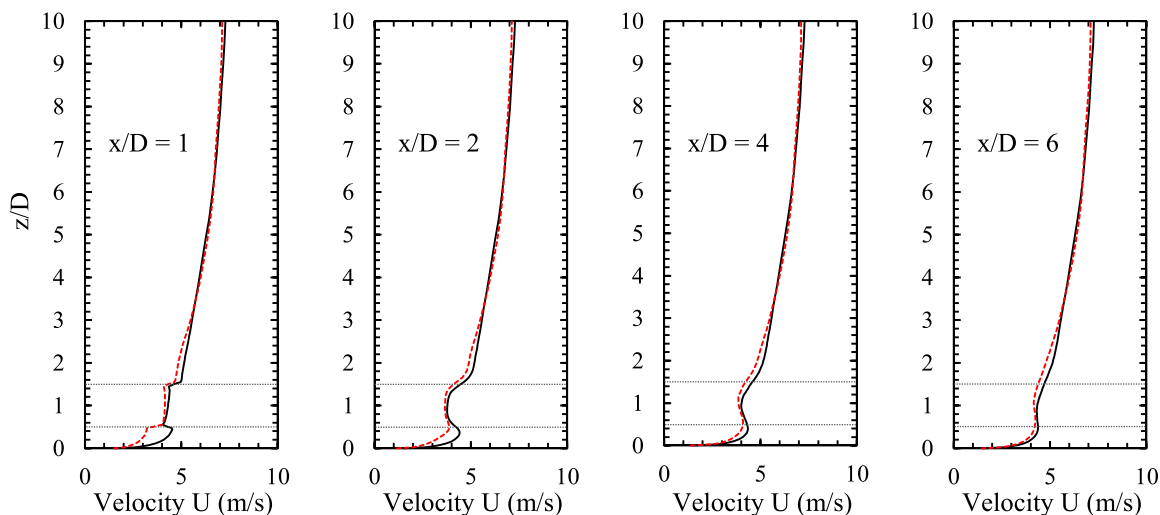


FIG. 16. Time-averaged streamwise velocity profiles behind one of the turbines. Black solid line: Case 1 (no towers, $K_s = 0$) and red dotted line: Case 4 (with towers, $K_s = 1.422$).

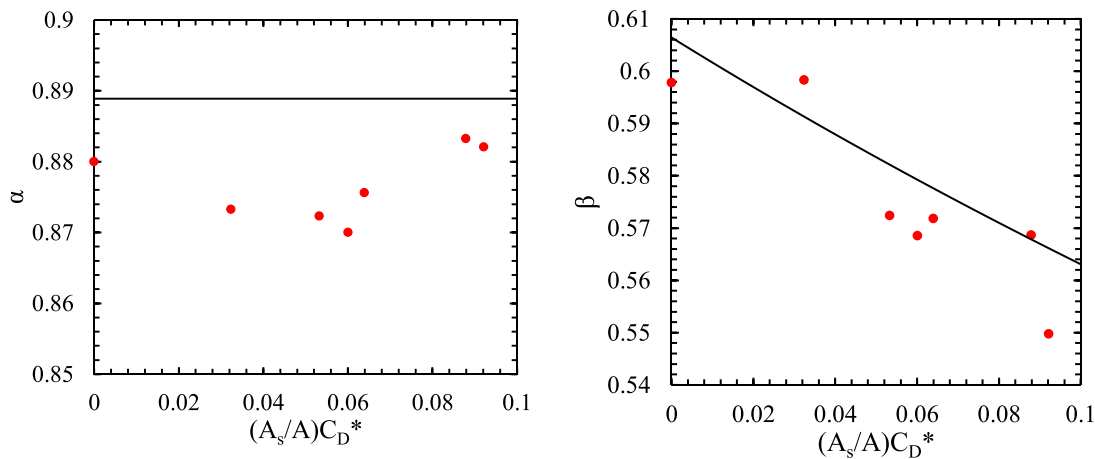


FIG. 17. Comparison of α (left) and β (right) between the CFD (red symbols) and theoretical model (black line).

on the overall farm performance as the farm density (or the number of turbines installed in a given farm area) increases. This is essentially because the optimal rotor thrust decreases, and therefore, the relative importance of support-structure drag increases as the farm density increases. In particular, for the case of an infinitely large wind farm, the proposed model predicts that the optimal interturbine spacing (to maximize the power density) depends on the support-structure drag or, more specifically, the normalized support-structure drag $(A_s/A)C_D^*$.

For the case of a finite-size wind farm, the proposed theoretical model requires an estimation of an environment dependent parameter, ζ , for a given wind farm environment. This parameter represents the response characteristics (or strength) of the driving force of flow over the finite-size wind farm. The prediction of the value of ζ is the scope of an ongoing research and is outside the scope of this paper. However, we have employed three different values of ζ (selected based on an earlier CFD study in Ref. 17) to investigate the impact of support-structure drag on the performance of three different

hypothetical wind farms. The results show that the support-structure drag may still play an important role in a large finite-size wind farm regardless of the exact value of ζ . However, the optimal farm density increases with the response strength of the driving force; hence, the optimal turbine spacing cannot be predicted without knowing the value of ζ . It is therefore crucial to estimate this environmental parameter carefully and accurately in the future.

A series of CFD simulations (WMLES) of a periodic staggered array of wind turbines (with both rotors and support structures modeled simply as streamwise momentum losses) has also been conducted for comparison with the theoretical model for the case of an infinitely large farm case. Seven different resistance (K_s) values are employed for the support structures (towers) with all other conditions unchanged. The results confirm that the average wind speed through the farm tends to decrease, and so does the power, as the level of support-structure drag increases. The maximum difference in the power predicted is about 10%, which is a reasonably good agreement, considering the complexity of this unsteady 3D flow problem and the simplicity of the steady quasi-1D theoretical model.

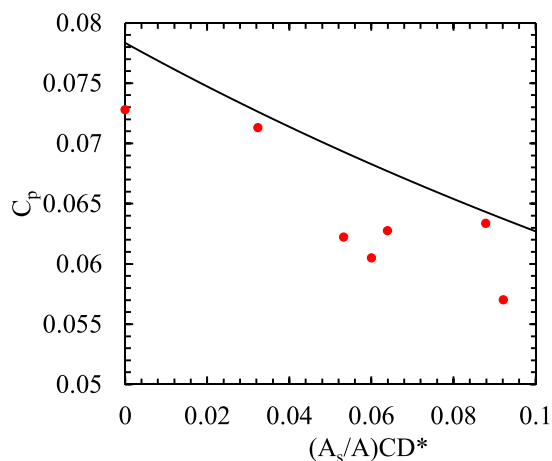


FIG. 18. Comparison of C_p between the CFD (red symbols) and theoretical model (black line).

REFERENCES

- ¹Ørsted, *Hornsea Project One & Two Offshore Wind Farms* (Ørsted, 2018).
- ²M. J. Churchfield, S. Lee, and P. J. Moriarty, "A large-eddy simulation of wind-plant aerodynamics," in 50th AIAA Aerospace Sciences Meeting, Nashville, TN, USA, 9–12 January (2012).
- ³A. Creech, W.-G. Früh, and E. Maguire, "Simulations of an offshore wind farm using large-eddy simulation and a torque-controlled actuator disc model," *Surv. Geophys.* **36**(3), 427–481 (2015).
- ⁴T. Chatterjee and J. Peet, "Exploring the benefits of vertically staggered wind farms: Understanding the power generation mechanisms of turbines operating at different scales," *Wind Energy* **22**(2), 283–301 (2019).
- ⁵M. Zhang, M. G. Arendshorst, and R. J. A. M. Stevens, "Large eddy simulations of the effect of vertical staggering in large wind farms," *Wind Energy* **22**(2), 189–204 (2019).
- ⁶Y.-T. Wu and F. Porté-Agel, "Large-eddy simulation of wind-turbine wakes: Evaluation of turbine parametrisations," *Boundary-Layer Meteorol.* **138**(3), 345–366 (2011).
- ⁷S. Frandsen, "On the wind speed reduction in the center of large clusters of wind turbines," *J. Wind Eng. Ind. Aerodyn.* **39**(1–3), 251–265 (1992).

- ⁸M. Calaf, C. Meneveau, and J. Meyers, "Large eddy simulation study of fully developed wind-turbine array boundary layers," *Phys. Fluids* **22**(1), 015110 (2010).
- ⁹C. Meneveau, "The top-down model of wind farm boundary layers and its applications," *J. Turbul.* **13**(7), 1–12 (2012).
- ¹⁰L. Ma and T. Nishino, "Preliminary estimate of the impact of support structures on the aerodynamic performance of very large wind farms," *J. Phys.: Conf. Ser.* **1037**, 072036 (2018).
- ¹¹T. Nishino, "Two-scale momentum theory for very large wind farms," *J. Phys.: Conf. Ser.* **753**, 032054 (2016).
- ¹²T. Nishino and W. Hunter, "Tuning turbine rotor design for very large wind farms," *Proc. R. Soc. A* **474**, 20180237 (2018).
- ¹³T. D. Dunstan, T. Muurai, and T. Nishino, "Validation of a theoretical model for large turbine array performance under realistic atmospheric conditions," in AMS 23rd Symposium on Boundary Layers and Turbulence, Oklahoma, OK, USA, 11–15 June (2018).
- ¹⁴A. Zapata, T. Nishino, and P.-L. Delafin, "Theoretically optimal turbine resistance in very large wind farms," *J. Phys.: Conf. Ser.* **854**, 012051 (2017).
- ¹⁵N. S. Ghaisas, A. S. Ghate, and S. K. Lele, "Farm efficiency of large wind farms: Evaluation using large eddy simulation," in 10th International Symposium on Turbulence and Shear Flow Phenomena, Chicago (2017).
- ¹⁶J. R. West and S. K. Lele, "Wind turbine performance in very large wind farms," in 71st Annual Meeting of the APS Division of Fluid Dynamics, Atlanta, USA, 18–20 November (2018).
- ¹⁷T. Nishino, "Generalisation of the two-scale momentum theory for coupled wind turbine/farm optimisation," in 25th National Symposium on Wind Engineering, Tokyo, Japan, December (2018).
- ¹⁸T. Nishino and S. Draper, "Theoretical prediction of the efficiency of very large turbine arrays: Combined effects of local blockage and wake mixing," in 7th Oxford Tidal Energy Workshop (OTE 2019), Oxford, UK, 8–9 April (2019).
- ¹⁹J. Meyers and C. Meneveau, "Optimal turbine spacing in fully developed wind farm boundary layers," *Wind Energy* **15**(2), 305–317 (2012).
- ²⁰W. M. Drennan, P. K. Taylor, and M. J. Yelland, "Parameterizing the sea surface roughness," *J. Phys. Oceanogr.* **35**(5), 835–845 (2005).
- ²¹S. K. Kanev, F. J. Savenije, and W. P. Engels, "Active wake control: An approach to optimize the lifetime operation of wind farms," *Wind Energy* **21**(7), 488–501 (2018).
- ²²S. Bhattacharya, "Challenges in design of foundations for offshore wind turbines," *Eng. Technol. Ref.* 1–9 (2014).
- ²³D. J. Tritton, *Physical Fluid Dynamics*, 2nd ed. (Clarendon Press, Oxford, 1988).
- ²⁴J. Blegg, M. Purcell, R. Ruisi, and E. Traiger, "Wind farm blockage and the consequences of neglecting its impact on energy production," *Energies* **11**(6), 1609 (2018).
- ²⁵K. L. Wu and F. Porté-Agel, "Flow adjustment inside and around large finite-size wind farms," *Energies* **10**(12), 2164 (2017).
- ²⁶T. Nishino and T. D. Dunstan, "Two-scale momentum theory for time-dependent modelling of large wind farms," [arXiv:1909.11449](https://arxiv.org/abs/1909.11449).
- ²⁷N. Tobin, A. Lavelly, S. Schmitz, and L. P. Chamorro, "Spatiotemporal correlations in the power output of wind farms: On the impact of atmospheric stability," *Energies* **12**(8), 1–12 (2019).
- ²⁸T. Chatterjee and J. T. Peet, "Contribution of large scale coherence to wind turbine power: A large eddy simulation study in periodic wind farms," *Phys. Rev. Fluids* **3**(3), 034601 (2018).
- ²⁹ANSYS Inc., *ANSYS Fluent User's Guide, Release 17.2*. (ANSYS Inc., 2016).
- ³⁰N. V. Nikitin, F. Nicoud, B. Wasistho, and K. D. Squires, "An approach to wall modeling in large-eddy simulations," *Phys. Fluids* **12**(7), 1629–1632 (2000).
- ³¹P. R. Spalart, S. Deck, M. L. Shur, K. D. Squires, M. K. Strelets, and A. Travin, "A new version of detached-eddy simulation, resistant to ambiguous grid densities," *Theor. Comput. Fluid Dyn.* **20**(3), 181–195 (2006).
- ³²B. Blocken, T. Stathopoulos, and J. Carmeliet, "CFD simulation of the atmospheric boundary layer: Wall function problems," *Atmos. Environ.* **41**(2), 238–252 (2007).
- ³³T. Nishino and S. Draper, "Local blockage effect for wind turbines," *J. Phys.: Conf. Ser.* **625**, 012010 (2015).